Open Access

Catalysis Research

LIDSEN Publishing Inc.

Original Research

Enhancing Kerosene Selectivity of Fischer-Tropsch Synthesis by Periodical Pore Drainage Via Hydrogenolysis

Carsten Unglaub, Andreas Jess *

University of Bayreuth, Chair of Chemical Engineering, Center of Energy Technology Universitätsstraße 30, 95447 Bayreuth, Germany; E-Mails: carsten.unglaub@uni-bayreuth.de; jess@uni-bayreuth.de

* **Correspondence:** Andreas Jess; E-Mail: jess@uni-bayreuth.de

Academic Editor: George Marnellos

Catalysis Research
2023, volume 3, issue 3
doi:10.21926/cr.2303022

Received: June 27, 2023
Accepted: September 06, 2023
Published: September 12, 2023

Abstract

Accumulation of wax inside the catalyst pores during transient cobalt-catalyzed Fischer-Tropsch synthesis (FTS) leads to unfavorable product distribution and low activity by imposing internal mass transfer limitations. The condensation of paraffin severely changes the apparent product stream that actually leaves the reactor before the catalyst pores are filled completely and the steady state is reached. Thus, the product distribution of the transient FTS is less complex than expected in comparison to the steady-state FTS and increasingly consists of hydrocarbons (HCs) with an average chain length in the range of kerosene (C_9-C_{17}). So, in order to prevent FTS from reaching a steady state, the pores are drained periodically by hydrogenolysis (HGL). The alternating HGL is realized by a switch from syngas (H_2, CO) to pure hydrogen at a reaction temperature in the range of 210°C to 240°C. The alternating process leads to an improvement in kerosene selectivity of 48%, 37%, and 28% at 210°C, 220°C and 240°C, respectively. Furthermore, the influence of temperature on the hydrogenolysis of long-chain HCs was experimentally investigated. It was found that temperature affects methane selectivity severely. A high hydrogenolysis temperature is favorable as this leads to a severely decreased overall methane selectivity and, thus to a higher production rate of alkanes within the carbon number range of 9 to 17.

Keywords
Hydrogenolysis; E-fuels; Fischer-Tropsch synthesis

1. Introduction

Since renewable energy sources such as biomass, wind, or sun are subject to strong seasonal and intersectional fluctuations, their intended expansion enhances the need for powerful, cost-effective, and efficient systems for the storage of electrical energy [1]. Batteries are expensive, have a limited capacity (heavy and bulky), and are not easy to recycle, which makes them today still not very suitable for large-scale storage. An alternative option is the chemical conversion of electricity into hydrogen by water electrolysis as the first step of storage and for further use of renewable electrical energy. Each conversion step in an overall process of utilization of (renewable) hydrogen reduces the overall efficiency. Thus, the chemical conversion of H_2 with carbon oxides (CO, CO_2) into liquid E-fuels such as methanol, diesel, or kerosene (jet fuel) by Fischer-Tropsch synthesis (FTS) is only feasible for certain (transport) applications: Chemical energy storage and utilization by FTS is energetically and economically only sensible for synthetic aviation fuels (SAF) or marine diesel oil, which require high energy density to achieve a long-range, and where also excellent stability for long-term storage even under adverse conditions is needed (no polymerization or degradation as for some biofuels) [2, 3].

On a large industrial scale, long-chain paraffins are now produced (apart from the components of crude oil) by low-temperature FTS (LTFT; 200-240°C) using natural gas or coal as feedstock. These paraffins are then further processed by mild hydrocracking to achieve an overall liquid fuel selectivity of up to 80%. For the production of lubricant base oils, hydroisomerization is usually employed [4, 5]. In addition, bifunctional co-zeolite catalysts have recently been successfully tested for the direct synthesis of liquid fuels from synthesis gas without intermediate wax formation or the need for additional reactors [6, 7]. During FTS, the hydrocarbon chains are formed by successive incorporation of carbon units and hydrogen into a hydrocarbon chain on the surface of the usually iron or cobalt-based catalyst. Thus, the FTS is often regarded as a heterogeneous catalyzed polymerization represented by [8]:

$$\mathrm{CO} + 2\mathrm{H_2} \rightarrow (-\mathrm{CH_2}-) + \mathrm{H_2O}\ \Delta_\mathrm{R}\mathrm{H}^0_{298} = -152\ \mathrm{kJ\ mol^{-1}} \quad (1)$$

The product distribution can be described by the Anderson Schulz-Flory (ASF) distribution using the chain growth probability α, Eq. (2). This gives an excellent approximation for the composition of hydrocarbons with a carbon number higher than three. The mass-based ASF distribution is given by Eq. (3).

$$\mathrm{x_n} = (1-\alpha)\alpha^{\mathrm{n}-1} \quad (2)$$

$$\mathrm{w_n} = \mathrm{n_n}(1-\alpha)^2\alpha^{\mathrm{n}-1} \quad (3)$$

Since the formation of methane is usually strongly underestimated (for cobalt-based catalysts), the selectivity of methane cannot be calculated by the ASF distribution. In the literature, the high

methane selectivity of FTS is often explained by a second mechanism for the formation of methane besides FTS [9, 10]. The value of α depends on the catalyst, reaction temperature, and reactant concentration(s). Already small variations of the value of α cause a severe shift in product selectivity and distribution. High values of α lead to a broad variety of products with high mean carbon numbers, whereas low α results in a narrow product distribution with low mean carbon numbers. In LTFTS (cobalt catalyzed) a chain growth probability of at least 0.85 is considered necessary to obtain good product selectivity of kerosene and diesel [11]. The chain growth probability can be obtained from experimental product distributions by the logarithmic form of Eq. (2), where log(α) represents the slope of the linear plot, Eq. (4) [8, 12]:

$$\log(x_n) = \log(1-\alpha) + (n-1)\log(\alpha) \quad (4)$$

The initial phase of LTFTS before reaching stationary operation is not fully understood and currently still investigated [11, 13-15]. Inside the catalyst pores long-chain hydrocarbons accumulate and eventually completely fill the porous system. Due to a higher mass transport resistance ($D_{gas} \approx 100\ D_{liq}$), the overall (effective) activity of the process is reduced [15]. Only initially, as long as the catalyst pores are practically empty, the FTS can be seen as a gas-solid reaction. In the further course of the reaction, wax accumulates inside the catalyst, and the characteristic of the reaction shifts to a three-phase reaction. Thus, a vapor liquid equilibrium has to be considered. During the filling of the pore, the diffusion length increases with increasing wax layer thickness, but mass transport via gas diffusion is still possible. As soon as the 'transportation' pores (macro pores) fill, the mass transport resistance increases substantially since syngas can then only be transported by diffusion via the liquid phase [11-13, 16-18]. Iglesia et al. reported that the catalyst structure, like particle diameter, porosity, surface density of metal, and pore diameter, severely affect product selectivity. The probability of olefin readsorption for example, increases with increasing catalyst diameter, leading initially to a higher selectivity to long-chain hydrocarbons (S_{C5+}). If the particle diameter increases, occurring CO transport limitations induce a decrease in S_{C5+}. Since CO diffuses much faster than C_{3+} olefins through liquid hydrocarbons the occurrence of diffusion limitations appears at large and more reactive catalyst pellets. CO depletion leads to low local CO concentration and high H_2/CO ratios at the catalytic site towards the center of the catalyst. These conditions lead to a high probability of chain termination and in consequence to high methane selectivity and low S_{C5+} [12, 19-21]. In order to reduce or avoid mass transport limitations eggshell type catalysts are often used in technical tube reactors. The catalysts in slurry or micro-structure reactors are also free of internal diffusion limitations since the particle sizes of 50-200 µm are too small [22]. However, the production of large amounts of water (by-product of FTS) can severely influence the product selectivity of the reaction. According to Hibbitts et al. water promotes chain growth by increasing the rate of formation of activated C_1 species without influencing the chain termination, leading to longer chains with high water partial pressure. Hence, high turnover rates can favor the production of long-chain hydrocarbons (S_{C5+}) [23].

Hydrogenolysis (HGL) of alkanes describes a cleavage reaction characterized by the breaking of C-C bonds in the presence of hydrogen, resulting in mostly linear alkanes with lower molar masses by eliminating short-chain alkanes, mainly methane. Hydrogenolysis does not have any industrial application, but has recently got attention among researchers as a possibility to efficiently degrade raw materials such as polyethylene (PE) [24, 25], polypropylene (PP) [26, 27], or lignin [28] to

methane and alkanes within the diesel and gasoline range. The first step in hydrogenolysis is the dissociative adsorption of hydrogen (Eq. (5)) on the catalyst surface and the initial break of the first C-H bond of the adsorbed alkane (Eq. (6) and Eq. (7)). The alkane is further dehydrogenated by successive cleavage of the C-H bond (Eq. (8)) until the C-C bond is weak enough to be cleaved (Eq. (9)) [29-31]. Flaherty et al. reported the need for cleavage of at least four hydrogen atoms from the alkane before the rupture of the C-C bond happens, and thermodynamic calculations suggest that the breaking of the C-H bonds most likely occurs on two vicinal carbon atoms [32, 33]. Thus, free adsorption sites are needed for the C-C bond activation, which causes the strong hindrance of hydrogenolysis by hydrogen. Frequently, a strong negative reaction order in the range of -2 to -3 about hydrogen is reported. However, the influence of hydrogen partial pressure depends strongly on temperature, alkane chain length, and alkane partial pressure. The reaction order of hydrogen becomes less negative with increasing temperature because, at high temperatures, the surface coverage of hydrogen is lower, resulting in less hindrance of the initial C-H bond rupture [34-40]. Long chain alkanes have a stronger interaction with the catalyst, facilitating dehydrogenation activation and stabilizing the transition state. Thus, the overall reaction rate of hydrogenolysis increases with alkane chain length and the maximum rate shifts to higher hydrogen pressures [32, 33, 35]. After the cleavage of the C-C bonds, C-H bonds reform, and the fragments of the alkane desorb (Eq. (10)). All steps including H-H or C-H dissociation are considered (quasi-) equilibrated. This renders the C-C bond braking the only kinetically relevant step [29]. According to Kempling and Anderson the product distribution of hydrogenolysis is governed by a combination of two processes: 1) predominantly but not exclusively cracking of the terminal C-C bond which produces mainly methane, and 2) the desorption of the remaining alkane chain. Hence the product selectivity depends mostly on the ratio of cracking rate and rate of desorption. The alkane is cracked as long as the remaining alkane is adsorbed. Thus, a high methane selectivity results from fast alkane cracking or slow desorption. The desorption rate is high in case of low conversion and thus, a low alkane partial pressure in the gas phase facilitates desorption or high temperature [37, 41].

$$\mathrm{H_2} + 2^* \rightleftarrows 2\,\mathrm{H}^* \tag{5}$$

$$C_nH_{2n+2} + 1^* \rightleftarrows {C_nH_{2n+2}}^* \tag{6}$$

$$\mathrm{C_nH_{2n+2}} + 1^* \rightleftarrows {\mathrm{C_nH_{2n+1}}}^* + \mathrm{H}^* \tag{7}$$

$${C_nH_{2n+2(y-1)}}^{\gamma *} + 1^* \rightleftarrows {C_nH_{2n+2-\gamma}}^{\gamma *} + H^* \tag{8}$$

$$\mathrm{C_nH_{2n+2-y}}^{\gamma *} \longrightarrow \mathrm{C_aH_{a'}}^{\mathrm{A}*} + \mathrm{C_bH_{b'}}^{\mathrm{B}*} \tag{9}$$

$$\mathrm{C_aH_{a'}}^{\mathrm{A}*} + \mathrm{x\,H}^* \rightleftarrows \mathrm{C_aH_{2a+2}} + (\mathrm{A} + \mathrm{x})^* \tag{10}$$

Deactivation of industrial supported cobalt catalyst is postulated to be due to oxidation of the elementary cobalt to inactive cobalt oxides, sintering of small cobalt crystallites and carbon or wax deposition. Thermodynamic calculations have shown that bulk cobalt oxidation to cobalt oxides is highly unlikely at common FT synthesis turnovers and conditions with crystallite sizes above 2 nm [42-45]. Reactivating the catalyst by repetitive removal of accumulated wax is not a new idea. In the early 1930s and 1940s, Otto Roelen at Ruhrchemie reported a successful reactivation procedure of deactivated cobalt catalyst by hydrogenation of the hydrocarbon deposits at around 200°C and at

0.75 bar hydrogen pressure [42, 46, 47]. More recently, the in-situ extraction of wax from the catalyst pores using supercritical or near-critical solvents had been proposed, what comes with the drawback for the need of high process pressure [48-50]. In order to maintain the high activity and the favorable product selectivity (low methane production rate) of the transient FTS, the (partially) filled catalyst pores are emptied periodically by hydrogenolysis (Figure 1).

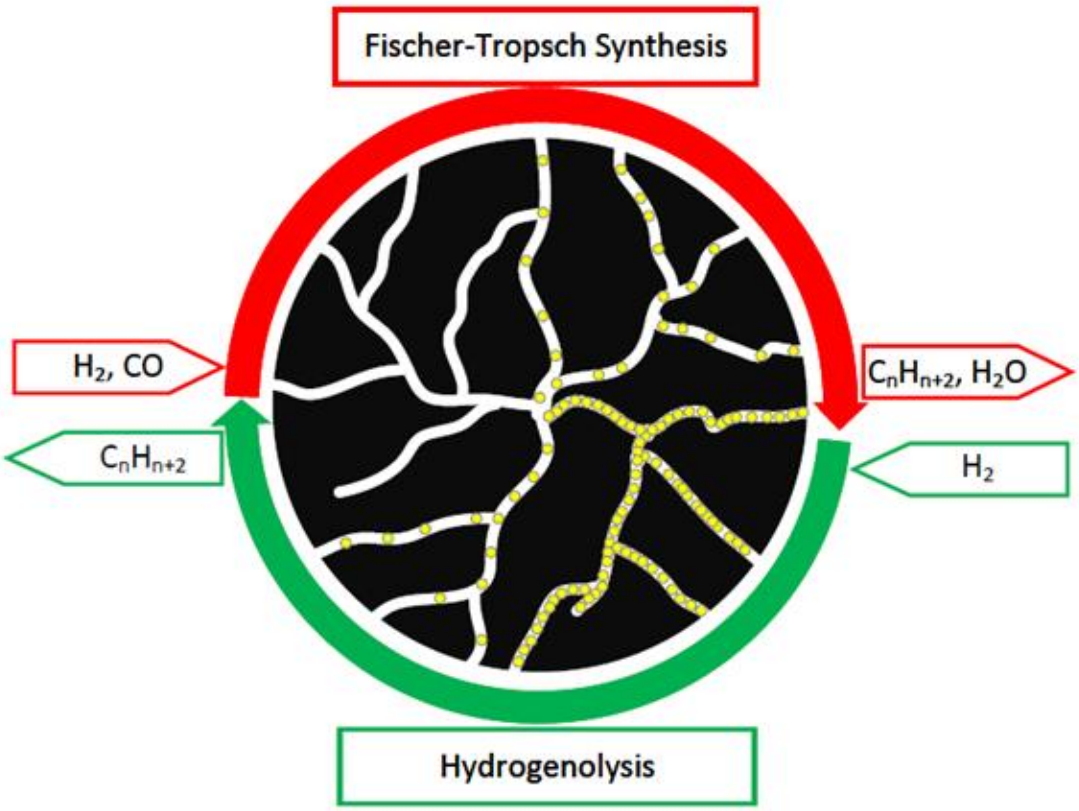

Figure 1 Schematic illustration of the concept of the alternating process consisting of pore filling with FTS and subsequent periodical pore drainage by hydrogenolysis after FTS. The building up of the wax layer is schematically indicated by yellow dots.

The proof of principle for the alternating process and its potential to improve overall activity and mean product selectivity has already been published by our group [51, 52]. For better comparability, Duerksen et al. introduced the process enhancement factor PE_{CO} to compare the total CO consumption of the alternating process with consumption in a steady state FTS) [51]. Therefore, the integral activity of the alternating operation is normalized to the FTS and HGL time and set about the stationary activity:

$$PE_{CO} = \frac{\int_0^{t_{FTS}} r_{CO}\, dt}{(t_{FTS} + t_{HGL})\, r_{CO,steady-state}} \qquad (11)$$

The higher the PE factor, the higher the (mean) activity of the alternating process compared the steady state. The shorter the drainage time t_{HGL} the higher the PE factor, and for $t_{HGL} \rightarrow 0$, $PE_{CO} \rightarrow 1/\eta_{pore}$. Later, PE_{C2+} was introduced to extend the concept of the process enhancement

factor to the production of valuable non-methane products (C_{2+}) [52]. Previously published PE factors of selected cycle times are presented in Table 1. From this it becomes obvious that the alternating process is capable of substantially increasing the productivity and decreasing overall methane selectivity over a vast variety of reaction temperatures and cycle times. Generally, the higher the reaction temperature, the higher the enhancement since mass transport limitations during steady-state FTS are more pronounced, and the hydrogenolysis activity is higher. Best results were achieved at 3 h of FTS reaction time at 240°C. However, the alternating process was shown to be effective at any tested temperature. So, it was possible to increase the overall activity up to 65% and the production rate of non-methane products up to 90% in comparison to the steady state FTS. This publication focuses lies primarily on the apparent product distribution of transient FTS and the influence of hydrogenolysis on the resulting kerosene selectivity of the alternating process. Therefore, the complex interplay between decreasing activity and chain growth probability α, alkane condensation and evaporation of the hydrocarbons while the pores are filling is investigated. In order to determine the optimum process conditions for the alternating process based not only on activity and methane production rate, but also for maximum kerosene (C_9-C_{17}) selectivity, a 20 wt.% cobalt (a typical cobalt content for industrial applications [53]) on Al_2O_3 catalyst is investigated in a temperature range between 210°C and 240°C. In addition, the influence of temperature on the selectivity of hydrogenolysis to minimize methane production is investigated. Finally, the kerosene selectivity of transient FTS and an alternating process is presented in comparison to the steady state FTS.

Table 1 Summary of previously published hydrogenolysis times, PE_{CO} and PE_{C2+} of selected FTS times in the temperature range of 210°C to 240°C [52]. The value of t_{HGL} refers to the time needed to fully drain the catalyst pores after 1 h, 3 h and 16 h on stream with FTS.

T_{FTS}/°C	t_{FTS}	1 h	3 h	16 h
	t_{HGL}/min	36	70	137
210	PE_{CO}/-	0.93	1.45	0.85
	PE_{C2+}/-	1.21	1.92	0.92
	t_{HGL}/min	47	67	81
220	PE_{CO}/-	1.02	1.55	0.95
	PE_{C2+}/-	0.67	1.42	0.93
	t_{HGL}/min	28	33	39
240	PE_{CO}/-	1.38	1.65	1.26
	PE_{C2+}/-	1.63	1.90	1.29

2. Experimental

2.1 Catalyst Preparation

For all experiments presented in this publication, a platinum (0.4 wt.%) promoted cobalt-Al_2O_3 catalyst with a cobalt content of 20 wt.% is used. The catalyst was synthesized by wet impregnation of 5 × 5 mm Al_2O_3 pellets from Sasol using cobalt(II)-nitrate-hexahydrate and tetraamineplatinum(II)-nitrate in water. After impregnation, the catalyst was dried at ambient

conditions for several days and then calcined by heating in air with a heating rate of 3 K/min to 340°C and a three-hour hold at that temperature. The specific pore volume of the catalyst is 0.39 cm^3/g and the mean pore diameter 7.9 nm. The metal content is measured with ICP-OES spectroscopy and for the BET-surface area nitrogen adsorption was employed. A summary of the catalyst characteristics is displayed in Table 2. Further characteristics of this catalyst can be found in Schurm et al. [54].

Table 2 Overview of the characteristic values of the catalyst and the support used in this work.

	Support	Catalyst
Cobalt content / wt%.	-	21.5
Platinum content / wt%.	-	0.04
BET surface area / m^2g^{-1}	190	148
specific pore volume / cm^3g^{-1}	0.55	0.39
Porosity	0.66	0.58
Geometry	5 × 5 mm cylinders	

2.2 Experimental Setup

All experiments were conducted in a continuous-flow fixed-bed reactor with an inner diameter of 14 mm, heated by an oil thermostat. For quick and easy exchange of the catalyst bed, the pellets were placed in an aluminum tube inlay with 8 mm inner diameter and a wall thickness of 3 mm. These dimensions were chosen to keep the inner diameter of the reactor smaller than two times the diameter of the used catalyst pellet ($d_{pellet} > 0.5\ d_{reactor}$), allowing a reliable determination of the axial position of each individual catalyst pellet. In order to handle the two strongly exothermic reactions of FTS and HGL the catalyst bed inside the aluminum inlay was diluted with stainless steel grist with a diameter of around 1 mm. To prevent the catalyst pellets from floating, the pellets were weighted down by 5 mm stainless steel beads placed between every catalyst particle. A more detailed description of the whole reactor concept can be found elsewhere [54].

2.3 General Proceedings

Before the first FTS run, the catalyst was activated by reduction with hydrogen (15 bar, 290°C, 16 h) and preconditioned by performing FTS at different temperature steps (up to the reaction temperature) for at least five hours. Every Fischer-Tropsch sequence was started with completely empty catalyst pores, and was initiated by replacing the H_2/N_2-feed gas (H_2/N_2 = 1/14; p = 15 bar) used for HGL by syngas (H_2/CO = 2/1; p = 15 bar) at the respective reaction temperature (210°C, 220°C, 240°C; "hot start"-conditions). Performing a hot start means exposing a completely "empty" catalyst to syngas at the designated reaction temperature, which is the most critical part of the procedure. This leads to a highly active FT synthesis, and the reactor temperature rose at maximum by 5°C for about 20 min at 240°C set temperature, for 210°C and 220°C maximum temperature deviation was not more than 2°C. The volume flow of syngas and the total amount of catalyst was adjusted to obtain a stationary CO conversion of 15%. But, due to the large deviation of the effectiveness factor during pore filling no exact specification of transient CO conversion can be given.

At 210°C, 220°C and 240°C the initial CO conversions (after the initial phase of 45 min) are 30%, 42%, and 50%, respectively (if conversion during the initial phase is considered, it can be as high as 65% at 240°C). To initiate the pore drainage by hydrogenolysis, the syngas feed was stopped and immediately replaced by a mixture of nitrogen and hydrogen (p_{H2} = 1 bar, p_{N2} = 14 bar, p_{total} = 15 bar, V = 45 l_{STP}/h). The pore draining reaction was considered as complete when the methane concentration in the product gas of HGL fell below 0.5 mmol kg_{Kat}^{-1} s^{-1}. No permanent deactivation of the catalyst was observed during any of the performed experiments [52]. Carbon monoxide consumption and methane selectivity of FTS were continuously monitored with a gas analyzer and a gas flow meter. The rate of consumption of CO was calculated according to Eq. (12). The rate of methane production can be calculated (Eq. 13) by ideal gas law using the volume share of methane (φ_{CH_4}) and the product volume flow ($\dot{V}_{out}$).

$$\mathrm{r_{CO}} = \frac{\dot{\mathrm{n}}_{\mathrm{CO,in}} - \dot{\mathrm{n}}_{\mathrm{CO,out}}}{\mathrm{m_{catalyst}}} \tag{12}$$

$$\mathrm{r}_{CH_4} = \frac{p_{atm}\varphi_{CH_4}\dot{V}_{out}}{\mathrm{m_{catalyst}RT}} \tag{13}$$

For analyzing gaseous FTS products, a gas collection tube in combination with a GC (PerkinElmer Clarus 690 with capillary columns CP-Sil PONA CB, internal standard cyclopropane) was used. Chain growth probability was calculated using the correlation of Rose [55]. There, α_{FTS} is calculated from the C_{5+}-selectivity. The correlation is validated for a chain growth probability between 0.6 and 0.9. The resulting product distribution was then calculated from chain growth probability using Eq. (3). Since the chain growth probability only leads to a weak approximation for methane, the methane production rate has to be factored out. Values for methane selectivity given in the following are therefore, always measured separately by gas analysis. The carbon-based production rate of C_{2+} alkanes is calculated using Eq. (14).

$$r_{C,alkane} = r_{CO,C2+} = r_{CO} - r_{CH4} \tag{14}$$

The total mass of carbon used for the production of alkanes at any given reaction time is calculated by integration of the molar $\mathrm{r_{C,alkane}}$:

$$\mathrm{m_{C,alkane}} = \int_0^{\mathrm{t_{FTS}}} \mathrm{r_{C,alkane}}\,\mathrm{dt} * \mathrm{M_C} \tag{15}$$

In order to obtain the mass of each individual alkane from the total mass of converted carbon using ASF, the product is assumed to be one infinite long alkane. The mass of the product alkane was calculated using Eq. (16) (with n_C:n_H = 1:2).

$$\mathrm{m_{CH2}} = \mathrm{m_{C,alkane}} + \frac{2 * \mathrm{m_{C,alkane}} * \mathrm{M_H}}{\mathrm{M_C}} \tag{16}$$

Individual alkanes deviate from the ideal monomer only by the mass of two hydrogen atoms. The higher the total mass of the alkane the lower the deviation. Therefore, the mass fraction of carbon of each alkane is calculated, Eq. (17), and normalized by the carbon mass fraction of the monomer.

Since methane is not considered in this calculation, the highest divergence is calculated to 7.2% with ethane. After that, the mass distribution of each individual alkane produced by FTS can be calculated using Eq. (18).

$$W_{C,i,j} = \frac{i * M_C}{i * M_C + j * M_H} \tag{17}$$

$$m_{alkane,FTS} = \frac{W_{C,CH2}}{W_{C,i,j=(2n+2)}} * m_{CH2} * w_{i,ASF} \tag{18}$$

Liquid hydrocarbons are obtained from the product stream by using a cooling trap cascade consisting of one high-temperature cooling trap (120°C) to obtain long-chain paraffin followed by one ice cooled trap (0°C) and one dry ice-cooled trap (-78°C) to remove the small alkanes from the product stream. Cooling traps are washed with toluene and analyzed by GC (internal standard cyclooctane). The mass of the accumulated wax inside the catalyst pore is measured using a thermobalance (TG). After the FTS, the reactor was cooled as fast as possible and then flushed with hydrogen before the catalyst pellets were removed from the reactor. Then the pellet was placed inside the TG, and hydrogenolysis was performed under 1 bar hydrogen pressure and temperatures between 240°C and 260°C for at least 3 h, until the catalyst mass was constant. The difference between the weight at the beginning and the end was accounted as wax (Δm_{TG}). Using Eq. (19), the deviation in mass and pore volume ($v_{s,pore}$) leads to the corresponding pore filling degree (F_{FTS}):

$$F_{FTS} = \frac{\Delta m_{TG}}{m_{cat,pellet} * v_{s,pore} * \rho_{wax}} \tag{19}$$

The composition of the accumulated wax in the catalyst after FTS was measured by extracting the wax with toluene in a Soxhlet extractor for 48 h at 73°C. The extracted samples were analyzed by GC (Varian CP-3800 with capillary columns Agilent VF-5ht UltiMetal, internal standard cyclooctane). Gaseous products of hydrogenolysis were collected using a 10 l inert foil gas sampling bag and liquid samples were collected using a cooled (0°C) scrubber filled with toluene and a cooling trap (-78°C) behind the scrubber. These specimens were also analyzed by GC (PerkinElmer Clarus 690 with capillary columns CP-Sil PONA CB, internal standard cyclopropane).

3. Results and Discussion

3.1 Transient Fischer-Tropsch Synthesis

Fischer-Tropsch synthesis performed with catalysts of industrial geometry with regard to limiting the pressure in fixed-bed reactors (diameters of 2-4 mm) suffers from poor pore effectiveness factors and high methane selectivity, both caused presumably by the accumulation of wax inside the porous system. Experiments on the influence of the particle size on the effective reaction rate conducted by our group using crushed particles (d_p < 150 µm) and whole particles (d_p = 1.6 mm) indicate the clear influence of pore diffusion on methane selectivity and activity [56]. It is also known in the literature that high water partial pressure can influence the selectivity of the FTS. High CO turnover the result in a high water production rate hence increase the S_{C5+} [23, 57]. A typical course of activity, chain growth probability, and methane selectivity over reaction time is presented in

Figure 2. During the initial phase, a distinct high activity along with an increase in reactor temperature (up to 4°C at 240°C, around 1°C at 210°C and 220°C) is observed for a short period of time. Then, the reaction 'calms down' quickly after the "hot-start". As the reaction progresses, the pore effectiveness factor and the chain growth probability decrease considerably due to the increase in the wax mass deposited within the catalyst pores (pore filling degree, Table 3). It is also conceivable that the significant decrease in chain growth probability is caused by the diminishing water partial pressure due to the decreasing activity. At least for our cobalt catalyst water (steam) only leads to the decline of conversion for a relatively high partial pressure of steam. The highest partial pressure of steam is here around 4 bar (CO conversion 50%, right at the beginning of the experiment), which reduces the activity by only 20% [58]. According to measurements done by Pöhlmann et al. using a magnet suspension balance, the development of the first wax layer is always extremely fast compared to the wax deposition rates later in the reaction. However, the pore-filling degree does not simply influence the diffusion linearly. Severe impact on activity becomes noticeable only when the catalyst is already filled to around 50%. At a pore-filling of over 80%, the (mesoporous) transport pores are filled and mass transport is mainly done exclusively by slow liquid phase diffusion ($D_{gas} \approx 100\ D_{liq}$) [15]. This corresponds well with the measured values of pore-filling degree presented in Table 3. There it can be seen that the catalyst is at least 30% filled after only 1 hour of FTS at every reaction temperature examined. Reaction rate and chain growth probability decrease as the pore-filling degree increases. Growth of the pore-filling slows down with reaction time. The pore-filling degrees above 100% at 210°C and 240°C after 100 h time on stream can be attributed to the fact that the wax starts to drip out of the catalyst pores and adhere to the catalyst surface, resulting in a pore-filling degree above the theoretical maximum. Theoretically, the decrease in activity can also be due to the deactivation of the catalyst (oxidation, sintering), since activity and CO turnover are very high. However, since in the literature the duration of deactivation to 50% of initial activity is often in the range of several days to months and the activity of the catalyst used here can be easily restored after a short treatment with hydrogenolysis (see chapter 3.2), it is very likely that the wax in the catalyst pores is the main cause of the activity decline [59].

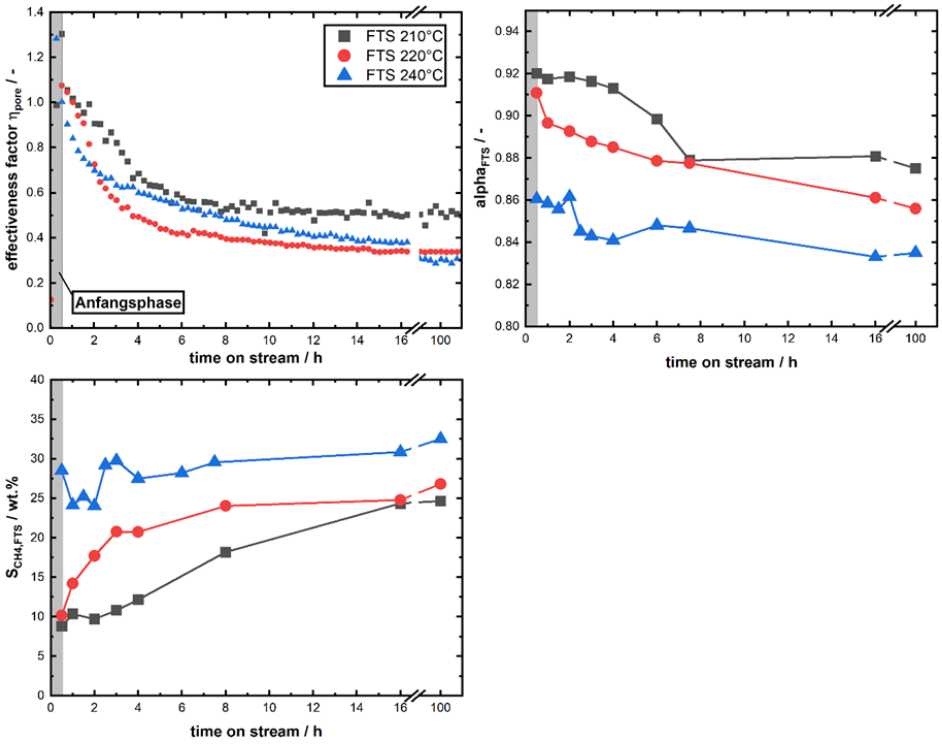

Figure 2 Typical course of activity, chain growth probability and methane selectivity with reaction time and variation of temperature. ($V_{syngas,\ 210\ °C}$ = 2.5 l_{STP} (g_{cat} h)$^{-1}$; $V_{syngas,\ 220\ °C}$ = 5 l_{STP} (g_{cat} h)$^{-1}$; $V_{syngas,\ 240\ °C}$ = 30 l_{STP} (g_{cat} h)$^{-1}$; p_{total} = 15 bar; H_2/CO = 2/1).

Table 3 Pore-filling degree after 1 h, 3 h and 16 h of reaction time at 210°C, 220°C and 240°C. In each of the 12 experiments of pore-filling, the catalyst was initially empty, that i.e. free of any liquid HCs (see 2.3 General Proceedings).

Temperature	Filling time by FTS			
In °C	1 h	3 h	16 h	100 h
210	33%	48%	96%	102%
220	53%	77%	92%	103%
240	36%	60%	84%	90%

At high reaction temperatures mass transport limitations are more present, leading to low stationary effectiveness factors. Thus, stationary effectiveness factors of 50%, 33%, and 29% are measured at 210°C, 220°C, and 240°C, respectively. The parallelly decreasing alpha value leads to a highly variable product distribution during the transient FTS and to a constant decrease in the molecular weight of the reaction products. The change in production rate and product distribution over time on stream make filling of the catalyst pores a complex issue. At 210°C the pore filling is slow despite the high alpha values because of low overall activity. At 240°C the activity is much higher, but the chain growth probability is much lower, resulting in comparably slow wax accumulation. The pores are filled most efficiently at 220°C. Since the amount of wax depends on reaction rate and chain growth probability as well as evaporation during the process, the pore filling degree is not independent from the wax composition. The composition of the wax extracted from the catalyst pellets after various hours on stream and reaction temperatures is depicted in Figure 3.

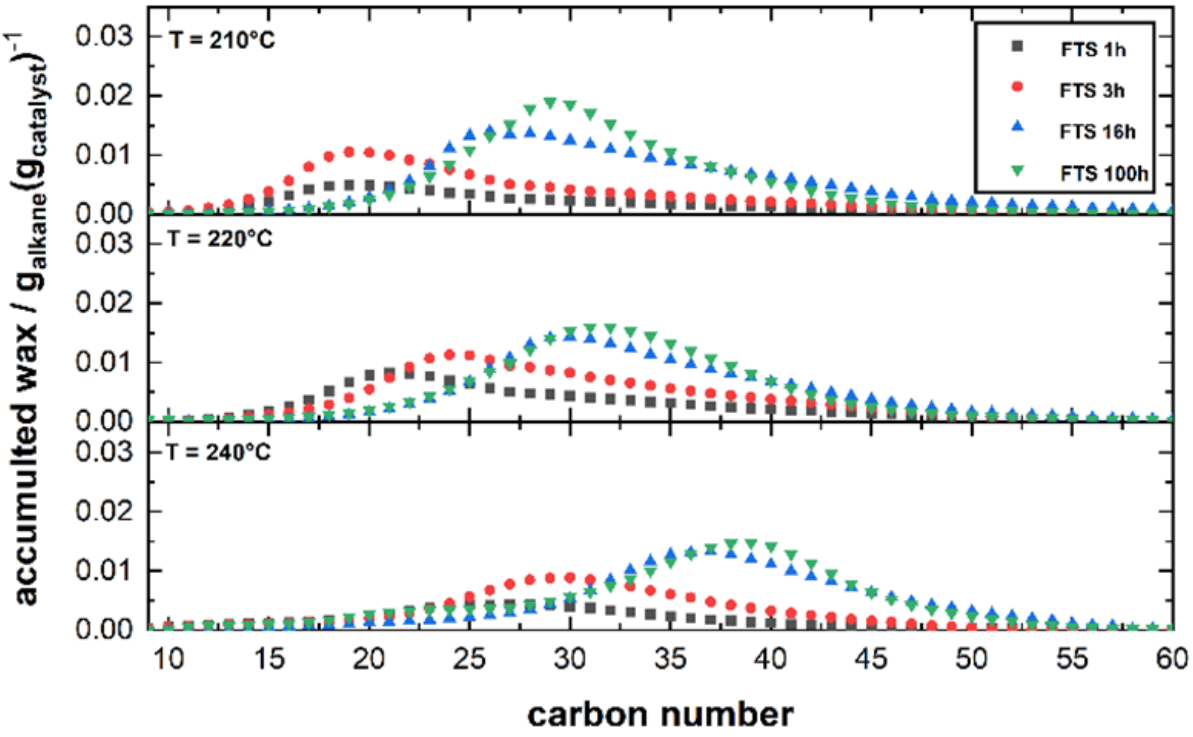

Figure 3 Transformation of the composition of the accumulated wax inside the catalyst pore with variation of synthesis time and temperature.

The mean carbon number increases with increasing temperature as evaporation is facilitated, even if the chain growth probability decreases. A longer reaction time has a similar effect as increased temperature. As the reaction time increases, the average carbon number increases because the evaporation time is longer, and the product partial pressure is lower due to the low efficiency that facilitates evaporation. Once the maximum pore filling degree is reached the hydrocarbon distribution changes only marginally with reaction time. These accumulated waxes are later cracked by hydrogenolysis. The complex interplay of alkane production and condensation during transient FTS at 220°C and its effect on the apparent FTS product stream leaving the reactor is depicted in Figure 4. The integral amount of each alkane (total FTS products) produced during the time of FTS (1 h, 3 h, 16 h) was calculated from carbon monoxide turnover and measured α - values (Table 3) by applying the equations (12) to (18). Integral α values are obtained by weighing the differential α by activity (Figure 2). The integral values of α are in excellent agreement with the catalyst pores. All alpha values are listed in Table 4.

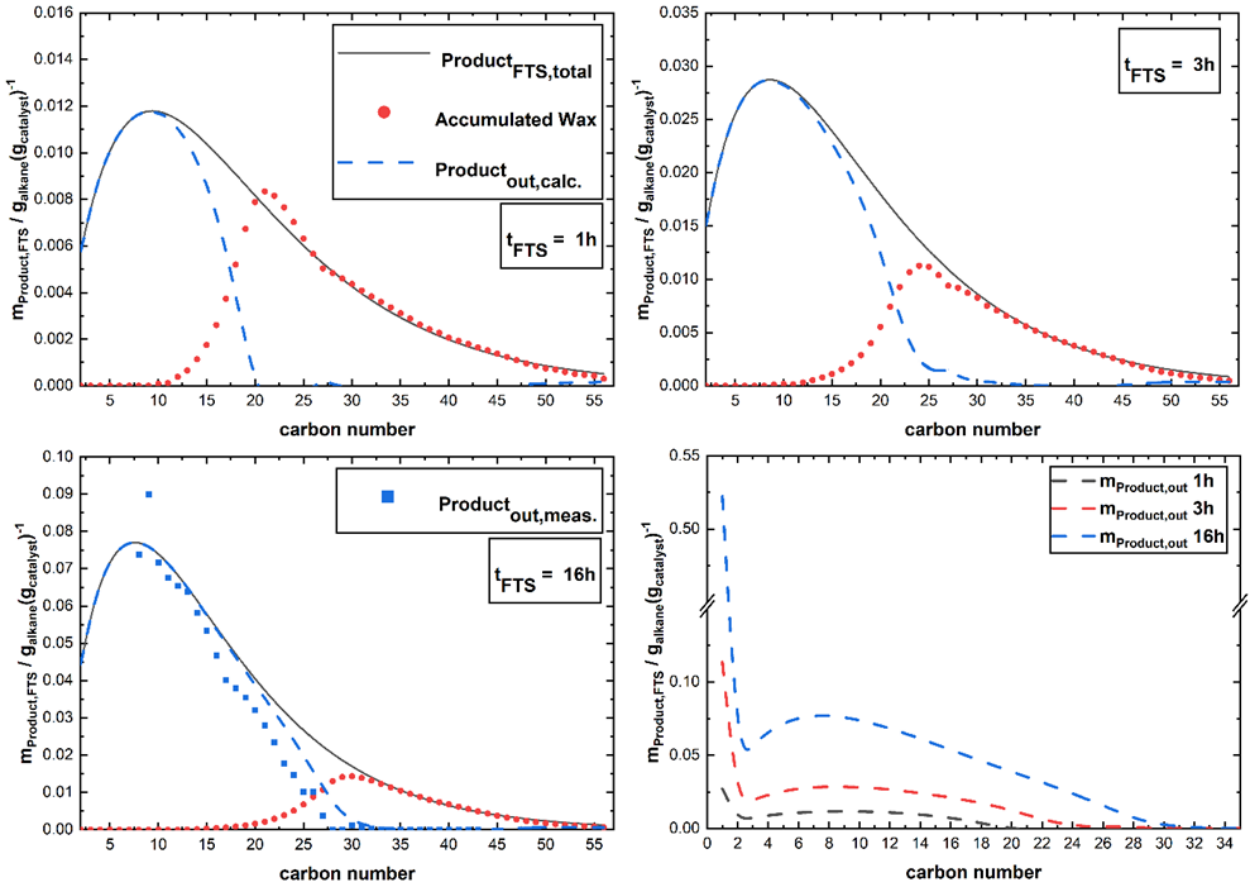

Figure 4 Depiction of calculated alkane production ($Product_{FTS,total}$) and apparent product stream ($Product_{out,calc}$) besides wax accumulation (Accumulated Wax) during transient FTS for 1 h, 3 h and 16 h reaction time at 220°C without considering methane. Calculated values are shown with lines, measured values with points. Apparent product distribution including methane (methane measured with a gas analyzer) is displayed in the bottom right figure.

Table 4 Comparison of total mass of alkanes produced during FTS (malkane, FTS) and deposited in the catalyst (mWax) of selected FTS times with maximum carbon number of apparent product stream. Comparison of chain growth probabilities of the gaseous products and the accumulated wax extracted from the catalyst pores.

T_{FTS} / °C	t_{FTS}	1 h	3 h	16 h
	$m_{alkane,FTS}$/ g_{HC}/g_{cat}	0.15	0.41	1.12
	m_{Wax} / g_{HC}/g_{cat}	0.09	0.13	0.26
210	$\alpha_{FTS,Gas,calc.}$ / -	0.92	0.92	0.90
	$a_{FTS,Wax}$ / -	0.91	0.89	0.89
	C_{max} / -	18	18	34
	$m_{alkane,FTS}$/ g_{HC}/g_{cat}	0.29	0.70	2.13
	m_{Wax} / g_{HC}/g_{cat}	0.14	0.20	0.24
220	$\alpha_{FTS,Gas,calc.}$ / -	0.90	0.90	0.88
	$a_{FTS,Wax}$ / -	0.89	0.88	0.87
	C_{max} / -	20	27	33

	$m_{alkane,FTS}$/ g_{HC}/g_{cat}	0.94	2.85	12.5
	m_{Wax} / g_{HC}/g_{cat}	0.09	0.15	0.21
240	$\alpha_{FTS,Gas,calc.}$ / -	0.86	0.86	0.84
	$a_{FTS,Wax}$ / -	0.86	0.84	0.84
	C_{max} / -	34	40	43

The apparent stream of products, which are volatile enough to leave the reactor, is calculated by subtracting the mass of the accumulated hydrocarbons from the mass of total produced alkanes during the FTS using Eq. (18).

$$m_{i,out} = m_{i,FTS} - m_{i,wax} \quad (18)$$

Comparing the calculated amount of total alkane produced with the amount of alkane accumulated in the catalyst, it becomes clear that above a specific chain length (usually the most common carbon number of the wax), all hydrocarbons produced condense altogether, thus significantly changing the product spectrum leaving the reactor (compared to steady-state FTS). As most of the high molecular hydrocarbons condense inside the catalyst pores the obtained product spectrum is of comparably short range despite the initially high chain growth probability. As the reaction proceeds the share of accumulated wax in the total formed product decreases since the catalyst pores can only fill with a certain amount of hydrocarbons corresponding to the pore volume. After 1 h FTS at 220°C, around 50% of the total product mass condenses inside the catalyst. At 16 h the fraction of accumulated wax is only 10%. This circumstance leads to the paradox fact that the maximum carbon number (C_{max}) of the product stream increases with time on stream despite severely decreased chain growth probability. The (almost) total catalyst pores can no longer hold so many hydrocarbons, which combined with the low alkane partial pressure in the gas phase (low activity), leads to an easier evaporation of alkanes with medium chain length.

This results in more medium-chain alkanes entering the product stream, which would otherwise have remained adsorbed with a shorter reaction time. The apparent product stream could only be measured at the longest reaction time of 16 h as otherwise, the reaction time is too short, and the total mass of products is too small. However, it is clearly visible that the measurement agrees with the calculated values. As can be seen in the bottom right of Figure 4, the total amount of product and the maximum carbon number of the alkane leaving the reactor increases along with the methane selectivity, resulting in a highly variable product stream. A summary of all relevant measures can be found in Table 3. The accumulated wax decreases with increased reaction temperature due to increased reaction activity but almost constant maximum hydrocarbon mass within the catalyst pores. The total mass of accumulated wax is limited to around 0.27 $g_{alkane}/g_{catalyst}$ whereas the total amount of produced alkanes during FTS is theoretically infinite. After 1 h of FTS the share of accumulated wax in the total mass of products is 60%, 48%, and 10% at 210°C, 220°C, and 240°C, respectively. Due to pronounced evaporation, the maximum carbon number traceable in the product stream increases with increasing temperature and reaction time.

3.2 Hydrogenolysis of Accumulated Waxes

In order to maintain the high activity and the favorable product distribution of the transient FTS, the catalyst pores are drained periodically by hydrogenolysis before the steady state (i.e. completely

filled pores) is reached. To start the HGL reaction, the syngas feed was stopped and immediately replaced by a mixture gas mixture consistent of nitrogen and hydrogen (p_{H2} = 1 bar, p_{N2} = 14 bar, p_{total}l = 15 bar). A typical course of methane productions rate during FTS and HGL at 240°C (after 16 h of FTS) is displayed in Figure 5. The figures of methane production rate after 1 h and 3 h of FTS at 240°C can be found in the Supplementary Information (Figure S1).

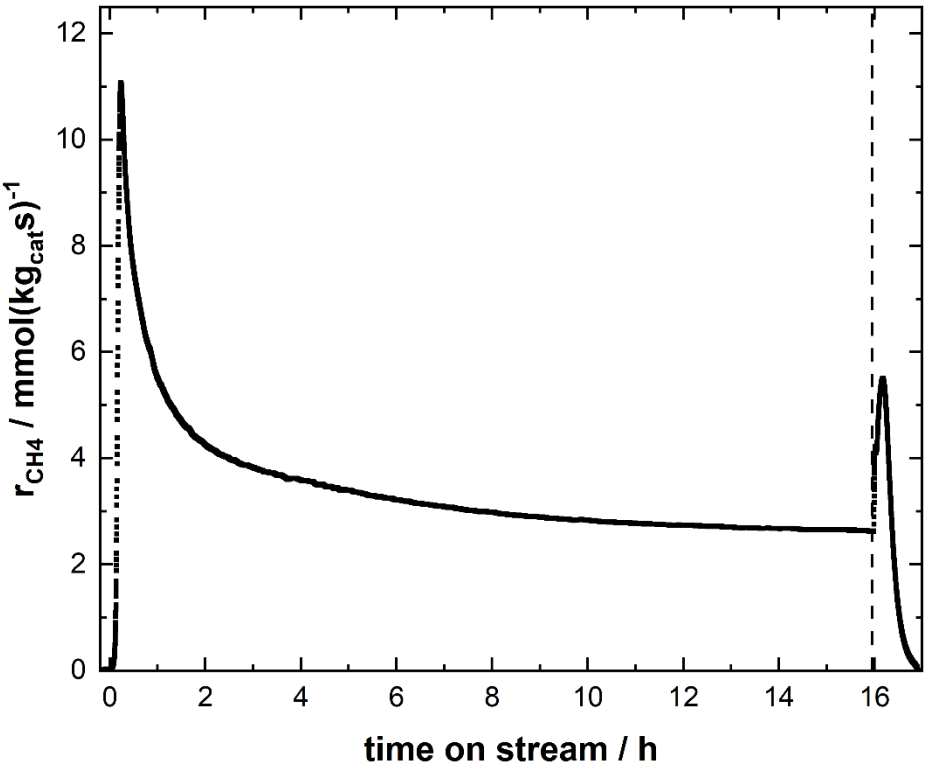

Figure 5 Typical course of methane production rate of FTS and subsequent HGL at 240°C after 16 h of FTS ($V_{syngas,\ 240°C}$ = 30 l_{STP} (g_{cat} h)$^{-1}$; H_2/CO = 2/1; $p_{total,\ FTS}$ = $p_{total,\ HGL}$ = 15 bar; $p_{H2,\ HGL}$ = 1 bar; $p_{N2,\ HGL}$ = 14 bar; $V_{gas,\ HGL,\ 240\ °C}$ = 45 l_{STP} (g_{cat} h).

Employing hydrogenolysis for cracking the accumulated waxes leads to conversion of C_{15}-C_{60} paraffins to C_1-C_{21} alkanes presumably improving the overall process selectivity of kerosene or products in the liquid fuel range. Hydrogenolysis is always performed at the same temperature and pressure as the previous FTS. The distribution of methane and the relevant product groups of light hydrocarbons (C_2-C_8) and hydrocarbons within the kerosene range (C_9-C_{17}) obtained from hydrogenolysis of the long chain hydrocarbons accumulated during FTS times of 1 h, 3 h and 16 h can be found in Table 5. Typically, products with carbon numbers of up to 21 can be found in the product stream but the proportion of products with a carbon number higher than 17 is usually less than 2% and is therefore neglected. The most abundant product of hydrogenolysis is always methane with a selectivity of up to 66 wt.% after 16 h FTS at 210°C. Methane selectivity grows with a reaction time of previously performed FTS. Longer time on stream results in, as mentioned before, a higher pore filling degree but also in a higher mean carbon number of the wax inside the pores. Thus, the effect causing the increase in methane selectivity remains unclear. Methane production is also influenced by temperature. Increasing hydrogenolysis temperature results in lower methane selectivity and substantially increased kerosene selectivity. The kerosene (C_9-C_{17}) selectivity increases from 16 wt.% at 210°C to 37 wt.% at 240°C. The kerosene selectivity is complementary to

the methane selectivity, whereas the selectivity of the lighter hydrocarbons (C_2-C_8) remains more stable over reaction time and temperature. However, since temperature also massively influences the composition of the accumulated hydrocarbons (Figure 3), no precise explanation for this effect can be given. The pores of the catalyst can be completely emptied at 240°C, while the pores at 210°C and 220°C still contain wax residues of about 10% to 20%. However, the residues could be completely removed at elevated temperature (240°C). No deactivation of the catalyst is observed, and FTS activity is always restored after pore draining (Supplementary Information, Figure S2). Even a high number of cycles, where pore filling and pore emptying alternate regularly, did not lead to any deactivation, even at a cycle number of 42 (at 210°C). A more detailed discussion of the hydrogenolysis of FTS waxes has already been published [52].

Table 5 Transformation of hydrogenolysis selectivity at various temperatures and FTS reaction time ($p_{H2,\ HGL}$ = 1 bar; $p_{N2,\ HGL}$ = 14 bar; $p_{total,\ FTS}$ = $p_{total,\ HGL}$ = 15 bar; $V_{gas,\ HGL,240°C}$ = 45 l_{STP} (g_{cat} h)).

T_{FTS} / °C	t_{FTS}	1 h	3 h	16 h
210	$S_{CH4,\ HGL}$ / wt.%	46.2	55.7	62.2
	$S_{C2\text{-}C8,\ HGL}$ / wt.%	21.1	16.1	19.1
	$S_{C9\text{-}C17,\ HGL}$ / wt.%	32.1	24.8	16.4
220	$S_{CH4,\ HGL}$ / wt.%	55.1	58.1	55.1
	$S_{C2\text{-}C8,\ HGL}$ / wt.%	18.7	18.4	19.0
	$S_{C9\text{-}C17,\ HGL}$/ wt.%	24.1	20.3	27.3
240	$S_{CH4,\ HGL}$ / wt.%	31.4	42.9	44.6
	$S_{C2\text{-}C8,\ HGL}$ / wt.%	12.4	14.4	17.9
	$S_{C9\text{-}C17,\ HGL}$ / wt.%	55.5	38.0	35.9

3.3 Influence of Temperature on Product Distribution of Hydrogenolysis

As described in the previous section 3.2, the hydrogenolysis product selectivity is severely influenced by temperature. Higher process temperature leads to decreased methane selectivity and higher kerosene selectivity (Table 4). According to *Kempling* and *Anderson* the hydrogenolysis proceeds by successive subtraction of small alkanes (mainly methane) as long as the remaining hydrocarbon stays adsorbed [41]. Increasing the reaction temperature promotes the evaporation of longer alkanes due to their resulting higher vapor pressure. Hence, the earlier terminated cracking reaction leads to lower methane selectivity. However, since both values of pore filling degree and composition of the FTS wax depend on temperature, no clear explanation for the influence of temperature on product distribution of hydrogenolysis can be given. In order to assess the influence of temperature on the system described here, the catalyst pores were always filled at 210°C for 1 h, 3 h or 16 h. Afterward hydrogenolysis was performed either directly at 210°C or the reactor was heated to 240°C under 15 bar hydrogen as fast as possible (t < 10 min). As the hydrogenolysis has a reaction order of -2 to -3 regarding hydrogen, the cracking during the heating is neglectable. Then, hydrogenolysis was performed as usual with a hydrogen partial pressure of 1 bar. The results are depicted in Figure 6. The product distribution presented there possesses the same characteristic shape often reported by other researchers [60-62]. The most common product is methane, with the product selectivity of the following hydrocarbons decreasing sharply until a

local maximum is reached at a carbon number of 7. Then the selectivity increases again until the local maximum at a carbon number of around 11 is reached. Thereupon selectivity decreases again. Alkanes with a chain length longer than 21 are not measured. It is obvious that a higher HGL temperature increases the C_9-C_{17} selectivity substantially. The methane selectivity severely decreases accordingly to 20 wt.%, 24 wt.%, and 50 wt.%, depending on the time of HGL (Figure 5, blank symbols), which is less than half the amount of methane formed at 210°C (HGL), at least for FTS times of 1 and 3 hours. The improvement in methane selectivity is less pronounced at a high pore-filling degree. Complementary, $S_{C9\text{-}C17}$ increases to 55 wt.%, 50 wt.% and 29 wt.% at 1 h, 3 h and 16 h time on stream, respectively. Thus, higher temperatures appear to be a viable way to increase the production of valuable non-methane products.

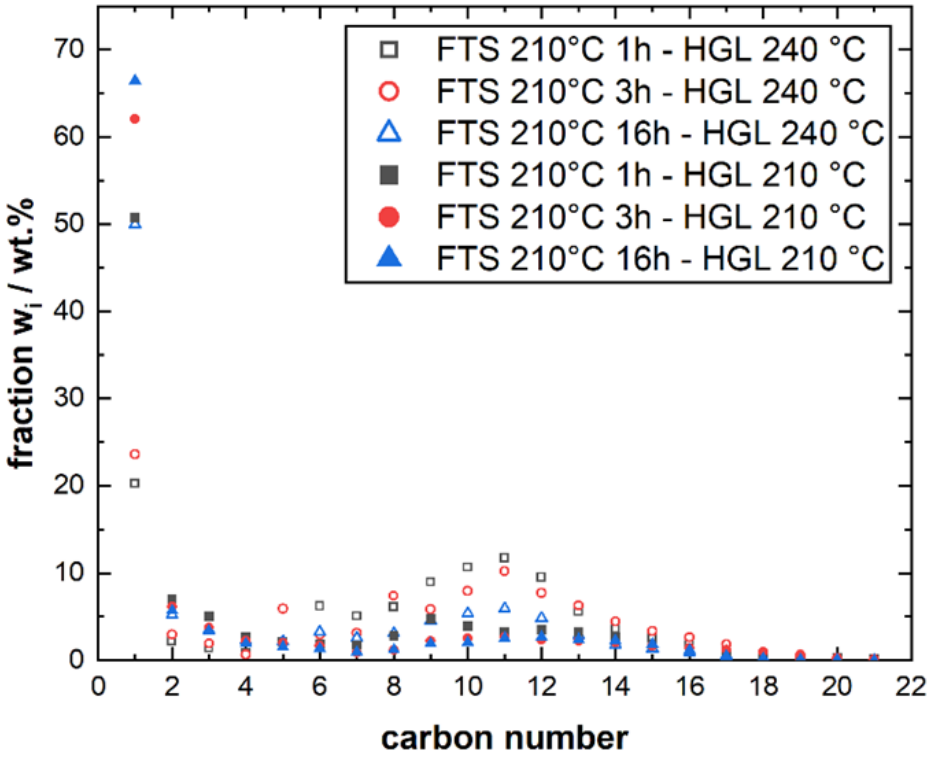

Figure 6 Representation of product selectivity of Hydrogenolysis at 210°C and 240°C after FTS at 210°C. Maximum measured hydrogen turnover during hydrogenolysis never exceeded 10%.

3.4 Selectivity of the Alternating Process to Kerosene (Jet Fuel)

To meet the required specifications for boiling behavior, stability, flash point, and freezing point, kerosene consists of a variety of olefins, paraffins, cycloalkanes and aromatic compounds. Kerosene of the JET-A standard contains, therefore, almost exclusively HCs with carbon numbers between 9 and 17 [63]. The selectivity of C_9-C_{17} (kerosene) of the transient FTS and the alternating process (AP) for the cycle times of 1 h, 3 h and 16 h is presented in comparison to the kerosene selectivity of the steady state FTS in Table 5. The apparent kerosene selectivity, calculated from products able to leave the reactor during transient FTS (Figure 4) is initially always significantly higher than the steady state one. The high-chain growth probability leads to a low amount of short-chain hydrocarbons and high product selectivity to heavy paraffins which easily condense within the catalyst pores

resulting in a high kerosene selectivity of the apparent product stream leaving the reactor. As the reaction progresses, the selectivities converge due to decreasing chain growth probability. Since the probability of chain growth also decreases with temperature apparently, the selectivity towards kerosene decreases with increasing reaction temperature leading to a less pronounced difference in product selectivity (transient product selectivity in comparison to steady state selectivity). It should also be noted that even at 100 h the pores are not completely filled at 240°C and the minor differences between the values measured at 16 h and 100 h (Table 3) leads to the conclusion that a substantially longer FTS time (if any) would be needed to fill the pores completely. Thus, the measurement done at 240°C after 100 h are considered as steady state. So, in order to maintain the favorable product selectivity of the transient FTS the pores have to be drained periodically by hydrogenolysis. As the reaction produces mainly alkanes in the C_9-C_{17} range in addition to methane, hydrogenolysis influences the overall selectivity of kerosene in the alternating process. The products of hydrogenolysis are added to the apparent product stream of the FTS to achieve the kerosene selectivity of the alternating process (AP). Since the alternating process is a combination of FTS/pore filling and of the subsequent HGL of the wax, the influence of hydrogenolysis on the overall selectivity of the alternating process depends on the ratio of the accumulated waxes to the total FTS product. During transient FTS, the ratio decreases, resulting in a smaller difference in product selectivity between the transient FTS and the alternating process. The same effect occurs with increasing temperature. The reaction rate rises severely with temperature, whereas the maximum amount of wax inside the catalyst pores remains almost constant. Hence, only a small impact of hydrogenolysis on total product distribution is notable. Nevertheless, the kerosene distribution of the alternating process is always improved, except for high pore filling degrees at 220°C. The highest kerosene selectivity with 41.4 wt.% is obtained at 210°C with a FTS time of 1 h, an increase of almost 50%. The alternating process carried out at 220°C showed similarly good results with 38.2 wt.% and 39.0 wt.%, an increase of around 40% compared to steady state at 1 h and 3 h. The alternating process at 240°C showed a maximum increase in kerosene selectivity of only 28 wt.%. At 240°C, the jet fuel selectivity of the alternating process is higher than that of the transient FTS due to the low methane selectivity of the hydrogenolysis. But, because of the low amount of accumulated wax relative to the total product mass, the impact on the total product distribution is low. If the alternating process is performed as described in section 3.3 (FTS 210°C - HGL 240°C) the kerosene selectivity could be further increased. The high accumulate to total product ratio in combination with the low methane selectivity of the high-temperature HGL result in kerosene selectivity of 52.8 wt.%, 44.1 wt.% and 36.1 wt.% for FTS time of 1 h, 3 h and 16 h, respectively. Kerosene selectivity obtained from transient FTS and alternating process (AP) after 1 h, 3 h and 16 h and the steady state FTS can be found in Table 6.

Table 6 Kerosene selectivity obtained from transient FTS, alternating process (AP) and the steady state FTS at selected synthesis time and temperature.

$T_{FTS,\ HGL}$ / °C	t_{FTS}	1 h	3 h	16 h
	$S_{C9\text{-}C17,\ FTS\text{-}trans.}$ / wt.%	50.1	42.1	36.0
210	$S_{C9\text{-}C17,\ AP}$ / wt.%	41.4	37.0	33.3
	$S_{C9\text{-}C17,\ FTS\text{-}stat.}$ / wt.%	27.7		
220	$S_{C9\text{-}C17,\ FTS\text{-}trans.}$ / wt.%	49.5	39.1	26.3

	$S_{C9\text{-}C17,\ AP}$ / wt.%	38.2	39.0	25.8
	$S_{C9\text{-}C17,\ FTS\text{-}stat.}$ / wt.%	27.8		
	$S_{C9\text{-}C17,\ FTS\text{-}trans.}$ / wt.%	30.6	30.0	28.8
240	$S_{C9\text{-}C17,\ AP}$ / wt.%	33.3	30.7	28.9
	$S_{C9\text{-}C17,\ FTS\text{-}stat.\ 100\ h}$ / wt.%	26.0		

4. Conclusions

The influence of mass transport restrictions during the time of transient FTS not only on activity and pore filling but also on overall product selectivity is investigated and discussed. Furthermore, the influence of temperature on HGL is examined. It has been found that the apparent product stream during transient FTS differs significantly from the expected product distribution due to the accumulation of the long chain hydrocarbon products within the catalyst pores. Despite of high alpha values, the hydrocarbons formed during transient FTS (in combination with HGL) have only relatively low carbon numbers of around 18 to 34 (at 210°C) or from 34 to 43 (at 240°C), depending on reaction time. Thus, the apparent selectivity towards kerosene can be as high as 51 wt.% (at 210°C, 1 h FTS) instead of 28 wt.% in the case of steady-state FTS. This effect can be used technically when hydrogenolysis is applied in order to prevent the FTS from reaching a steady state. Variations in hydrogenolysis temperature showed a clear dependence of methane selectivity on temperature. The higher the temperature, the lower the methane selectivity and the higher the C_9-C_{17} selectivity. The alternating process (FTS followed by hydrogenolysis) has been shown to improve the overall selectivity of the kerosene to a maximum value of 41.4 wt.% (at 210°C, 1 h FTS) without the need for an additional catalyst or further processes. If, additionally, the hydrogenolysis temperature is increased from a lower FTS reaction temperature, the kerosene selectivity can be improved even more (up to 52.8 wt.% for 1 h FTS 210°C - HGL 240°C). The alternating drainage of the wax-filled catalyst pores and hydrogenolysis after FTS thus not only have a positive effect on the activity and methane selectivity (Table 1), but also improve the kerosene selectivity of the FTS.

Acknowledgments

The authors gratefully acknowledge the financial support of this work by the German Research Foundation (Je 257/23-2).

Author Contributions

C. Unglaub: investigation, formal analysis, methodology, visualization; A. Jess: conceptualization, methodology, supervision, funding acquisition. All the authors discussed the results and contributed to the writing of the manuscript.

Competing Interests

The authors have declared that no competing interests exist.

Additional Materials

1. Figure S1: Typical course of methane production rate of FTS and HGL at 240°C after 1 h (left) and 3 h (right) of FTS ($V_{syngas,\ 240\ °C}$ = 30 l_{STP} $(g_{cat}\ h)^{-1}$; H_2/CO = 2/1; $p_{total,\ FTS}$ = $p_{total,\ HGL}$ = 15 bar; $p_{H2,\ HGL}$ = 1 bar; $p_{N2,\ HGL}$ = 14 bar).

2. Figure S2: Comparison of FTS activities before and after pore draining using Hydrogenolysis at 210°C, 220°C and 240°C after 16 h FTS. FTS run A is measured prior to pore drainage, whereas FTS run B is measured directly after the pore drainage. Adapted from [52].

References

1. Müller K. Technologies for the storage of hydrogen. Part 1: Hydrogen storage in the narrower sense. Chem Ing Tech. 2019; 91: 383-392.
2. Gallo AB, Simões Moreira JR, Costa HK, Santos MM, Dos Santos EM. Energy storage in the energy transition context: A technology review. Renew Sustain Energy Rev. 2016; 65: 800-822.
3. Müller K. Technologies for the storage of hydrogen. Part 2: Irreversible conversion and comparison of technologies. Chem Ing Tech. 2019; 91: 393-402.
4. Gregor JH. Fischer-Tropsch products as liquid fuels or chemicals: An economic evaluation. Catal Lett. 1990; 7: 317-331.
5. Kaiser P, Unde RB, Kern C, Jess A. Production of liquid hydrocarbons with CO_2 as carbon source based on reverse water-gas shift and Fischer-Tropsch synthesis. Chem Ing Tech. 2013; 85: 489-499.
6. Boymans E, Nijbacker T, Slort D, Grootjes S, Vreugdenhil B. Jet fuel synthesis from syngas using bifunctional cobalt-based catalysts. Catalysts. 2022; 12: 288.
7. Sartipi S, Parashar K, Valero Romero MJ, Santos VP, Van Der Linden B, Makkee M, et al. Hierarchical H-ZSM-5-supported cobalt for the direct synthesis of gasoline-range hydrocarbons from syngas: Advantages, limitations, and mechanistic insight. J Catal. 2013; 305: 179-190.
8. Jess A, Wasserscheid P. Chemical technology: An integral textbook. Weinheim: Wiley-VCH; 2013.
9. Botes FG. Proposal of a new product characterization model for the iron-based low-temperature Fischer-Tropsch synthesis. Energy Fuels. 2007; 21: 1379-1389.
10. Den Breejen JP, Radstake PB, Bezemer GL, Bitter JH, Frøseth V, Holmen A, et al. On the origin of the cobalt particle size effects in Fischer-Tropsch catalysis. J Am Chem Soc. 2009; 131: 7197-7203.
11. Pöhlmann F, Jess A. Interplay of reaction and pore diffusion during cobalt-catalyzed Fischer-Tropsch synthesis with CO_2-rich syngas. Catal Today. 2016; 275: 172-182.
12. Vervloet D, Kapteijn F, Nijenhuis J, Van Ommen JR. Fischer-Tropsch reaction-diffusion in a cobalt catalyst particle: Aspects of activity and selectivity for a variable chain growth probability. Catal Sci Technol. 2012; 2: 1221-1233.
13. Rößler S, Kern C, Jess A. Accumulation of liquid hydrocarbons during cobalt-catalyzed Fischer-Tropsch synthesis-influence of activity and chain growth probability. Catal Sci Technol. 2019; 9: 4047-4054.
14. Rößler S, Kern C, Jess A. Sorption and condensation of higher hydrocarbons in a Fischer-Tropsch catalyst. Catal Sci Technol. 2019; 9: 1902-1910.
15. Pöhlmann F, Kern C, Rößler S, Jess A. Accumulation of liquid hydrocarbons in catalyst pores during cobalt-catalyzed Fischer-Tropsch synthesis. Catal Sci Technol. 2016; 6: 6593-6604.

16. Van Der Laan GP, Beenackers AA. Kinetics and selectivity of the Fischer-Tropsch synthesis: A literature review. Catal Rev. 1999; 41: 255-318.
17. Anderson JR, Boudart M. Catalysis-science and technology [vol 1]. New York, NY: Springer-Verlag; 1981.
18. Huff Jr GA, Satterfield CN. Liquid accumulation in catalyst pores in a Fischer-Tropsch fixed-bed reactor. Ind Eng Chem Process Des Dev. 1985; 24: 986-995.
19. Iglesia E, Reyes SC, Madon RJ, Soled SL. Selectivity control and catalyst design in the Fischer-Tropsch synthesis: Sites, pellets, and reactors. In: Advances in catalysis. Amsterdam, Netherlands: Elsevier; 1993. pp. 221-302.
20. Pöhlmann F, Jess A. Influence of syngas composition on the kinetics of Fischer-Tropsch synthesis of using cobalt as catalyst. Energy Technol. 2016; 4: 55-64.
21. Kruit KD, Vervloet D, Kapteijn F, van Ommen JR. Selectivity of the Fischer-Tropsch process: Deviations from single alpha product distribution explained by gradients in process conditions. Catal Sci Technol. 2013; 3: 2210-2213.
22. Rytter E, Tsakoumis NE, Holmen A. On the selectivity to higher hydrocarbons in Co-based Fischer-Tropsch synthesis. Catal Today. 2016; 261: 3-16.
23. Hibbitts DD, Loveless BT, Neurock M, Iglesia E. Mechanistic role of water on the rate and selectivity of Fischer-Tropsch synthesis on ruthenium catalysts. Angew Chem Int Ed. 2013; 52: 12273-12278.
24. Celik G, Kennedy RM, Hackler RA, Ferrandon M, Tennakoon A, Patnaik S, et al. Upcycling single-use polyethylene into high-quality liquid products. ACS Cent Sci. 2019; 5: 1795-1803.
25. Ertem SP, Onuoha CE, Wang H, Hillmyer MA, Reineke TM, Lodge TP, et al. Hydrogenolysis of linear low-density polyethylene during heterogeneous catalytic hydrogen-deuterium exchange. Macromolecules. 2020; 53: 6043-6055.
26. Dufaud V, Basset JM. Catalytic hydrogenolysis at low temperature and pressure of polyethylene and polypropylene to diesels or lower alkanes by a zirconium hydride supported on silica-alumina: A step toward polyolefin degradation by the microscopic reverse of Ziegler-Natta polymerization. Angew Chem Int Ed. 1998; 37: 806-810.
27. Nakaji Y, Tamura M, Miyaoka S, Kumagai S, Tanji M, Nakagawa Y, et al. Low-temperature catalytic upgrading of waste polyolefinic plastics into liquid fuels and waxes. Appl Catal B. 2021; 285: 119805.
28. Jiang L, Guo H, Li C, Zhou P, Zhang Z. Selective cleavage of lignin and lignin model compounds without external hydrogen, catalyzed by heterogeneous nickel catalysts. Chem Sci. 2019; 10: 4458-4468.
29. Flaherty DW, Hibbitts DD, Gürbüz EI, Iglesia E. Theoretical and kinetic assessment of the mechanism of ethane hydrogenolysis on metal surfaces saturated with chemisorbed hydrogen. J Catal. 2014; 311: 350-356.
30. Frennet A, Lienard G, Crucq A, Degols L. Effect of multiple sites and competition in adsorption on the kinetics of reactions catalyzed by metals. J Catal. 1978; 53: 150-163.
31. Flaherty DW, Hibbitts DD, Iglesia E. Metal-catalyzed C-C bond cleavage in alkanes: Effects of methyl substitution on transition-state structures and stability. J Am Chem Soc. 2014; 136: 9664-9676.
32. Hibbitts DD, Flaherty DW, Iglesia E. Effects of chain length on the mechanism and rates of metal-catalyzed hydrogenolysis of n-alkanes. J Phys Chem C. 2016; 120: 8125-8138.

33. Flaherty DW, Iglesia E. Transition-state enthalpy and entropy effects on reactivity and selectivity in hydrogenolysis of n-alkanes. J Am Chem Soc. 2013; 135: 18586-18599.
34. Guczi L, Frennet A, Ponec V. Kinetics of hydrocarbon reactions on metals. Acta Chim Acad Sci Hung. 1983; 112: 127-151.
35. Bond GC. Kinetic modeling of metal-catalyzed reactions of alkanes. Ind Eng Chem Res. 1997; 36: 3173-3179.
36. Paâl Z. Hydrogen effects as a possible cause of inverse Arrhenius plots. J Catal. 1985; 91: 181-182.
37. Bond GC. Metal-catalysed reactions of hydrocarbons. Fundamental and applied catalysis. New York, NY: Springer; 2005.
38. Sinfelt JH, Taylor WF, Yates DJ. Catalysis over supported metals. III. Comparison of metals of known surface area for ethane hydrogenolysis. J Phys Chem. 1965; 69: 95-101.
39. Sinfelt JH. Kinetics of ethane hydrogenolysis. J Catal. 1972; 27: 468-471.
40. Sinfelt JH, Yates DJ. Catalytic hydrogenolysis of ethane over the noble metals of Group VIII. J Catal. 1967; 8: 82-90.
41. Kempling JC, Anderson RB. Kinetics of hydrogenolyses of n-Butane and Isobutane on supported ruthenium. Ind Eng Chem Process Des Dev. 1972; 11: 146-151.
42. Saib AM, Moodley DJ, Ciobîcă IM, Hauman MM, Sigwebela BH, Weststrate CJ, et al. Fundamental understanding of deactivation and regeneration of cobalt Fischer-Tropsch synthesis catalysts. Catal Today. 2010; 154: 271-282.
43. Van Berge PJ, Van de Loosdrecht J, Barradas S, Van Der Kraan AM. Oxidation of cobalt based Fischer-Tropsch catalysts as a deactivation mechanism. Catal Today. 2000; 58: 321-334.
44. Van de Loosdrecht J, Balzhinimaev B, Dalmon JA, Niemantsverdriet JW, Tsybulya SV, Saib AM, et al. Cobalt Fischer-Tropsch synthesis: Deactivation by oxidation? Catal Today. 2007; 123: 293-302.
45. Hilmen AM, Schanke D, Hanssen KF, Holmen A. Study of the effect of water on alumina supported cobalt Fischer-Tropsch catalysts. Appl Catal A. 1999; 186: 169-188.
46. British Intelligence Objectives Sub-Committee. Interrogation of Dr. Otto Roelen of Ruhrchemie A.G. London, UK: B.I.O.S.; 1945.
47. Emmett PH. Catalysis IV. Hydrocarbon synthesis, hydrogenation and cyclization. New York: Reinhold; 1956.
48. Jacobs G, Chaudhari K, Sparks D, Zhang Y, Shi B, Spicer R, et al. Fischer-Tropsch synthesis: Supercritical conversion using a Co/Al_2O_3 catalyst in a fixed bed reactor. Fuel. 2003; 82: 1251-1260.
49. Bochniak DJ, Subramaniam B. Fischer-Tropsch synthesis in near-critical n-hexane: Pressure-tuning effects. AIChE J. 1998; 44: 1889-1896.
50. Fan L, Fujimoto K. Fischer-Tropsch synthesis in supercritical fluid: Characteristics and application. Appl Catal A. 1999; 186: 343-354.
51. Duerksen A, Thiessen J, Kern C, Jess A. Fischer-Tropsch synthesis with periodical draining of a liquid-filled catalyst by hydrogenolysis. Sustain Energy Fuels. 2020; 4: 2055-2064.
52. Unglaub C, Tiessen J, Jess A. Enhancement of fischer-tropsch synthesis by periodical draining of the wax-filled pores of a cobalt catalyst by hydrogenolysis. Catal Res. 2023; 3: 001.
53. Van de Loosdrecht J, Botes FG, Ciobica IM, Ferreira AC, Gibson P, Moodley DJ, et al. Fischer-Tropsch synthesis: Catalysts and chemistry. Compr Inorg Chem. 2013; 7: 525-557.

54. Schurm L, Kern C, Jess A. Accumulation and distribution of higher hydrocarbons in the pores of a cobalt catalyst during low-temperature Fischer-Tropsch fixed-bed synthesis. Catal Sci Technol. 2021; 11: 6143-6154.
55. Rose A. Nano-carbon supported cobalt catalysts in Fischer-Tropsch synthesis. Bayreuth, Germany: Universität Bayreuth; 2013.
56. Kaiser P, Pöhlmann F, Jess A. Intrinsic and effective kinetics of cobalt-catalyzed fischer-tropsch synthesis in view of a power-to-liquid process based on renewable energy. Chem Eng Technol. 2014; 37: 964-972.
57. Iglesia E, Hibbitts D. The fischer-tropsch synthesis: A few enduring mechanistic conundrums revisited. J Catal. 2022; 405: 614-625.
58. Pöhlmann F. Interplay of chemical reaction and pore diffusion in cobalt-catalysed fischer-tropsch synthesis using synthesis gas containing CO_2. Bayreuth, German: University Bayreuth; 2016.
59. van de Loosdrecht J, Ciobica IM, Gibson P, Govender NS, Moodley DJ, Saib AM, et al. Providing fundamental and applied insights into fischer-tropsch catalysis: Sasol-eindhoven university of technology collaboration. ACS Catal. 2016; 6: 3840-3855.
60. Kuz'min AE, Kulikova MV, Dement'eva OS. Hydrogenolysis of alkanes in a three-phase slurry reactor over cobalt Fisher-Tropsch catalysts: A new product distribution model. Pet Chem. 2018; 58: 557-563.
61. Kulikova MV, Dement'eva OS, Kuz'min AE, Chudakova MV. Fischer-Tropsch synthesis and hydrogenolysis of long-chain alkanes over cobalt-containing nanosized catalysts in a slurry reactor. Pet Chem. 2016; 56: 1140-1153.
62. Nakaji Y, Nakagawa Y, Tamura M, Tomishige K. Regioselective hydrogenolysis of alga-derived squalane over silica-supported ruthenium‐vanadium catalyst. Fuel Process Technol. 2018; 176: 249-257.
63. Peters R. Fuel cell systems in aviation. Heidelberg, Germany: Springer Berlin Heidelberg; 2015.